Electrochemical performance of intermediate temperature micro-tubular solid oxide fuel cells using porous ceria barrier layers

M.J. López-Robledo[1,2,*], M.A. Laguna-Bercero[1], J. Silva[1], V.M. Orera[1], A. Larrea[1]

[1] *Instituto de Ciencia de Materiales de Aragón, CSIC-Universidad de Zaragoza, c/Pedro Cerbuna nº 12, 50009 Zaragoza, Spain*

[2] *Centro Universitario de la Defensa, General Military Academy, Ctra. Huesca s/n, 50090 Zaragoza, Spain*

** Corresponding author: Dr. Manuel Jesús López Robledo*

Email ID: robledo@unizar.es

Phone No.: +34 976 73 98 45, ext. 6945;

Fax: +34 976 73 98 24

Abstract

We describe the manufacture and electrochemical characterization of micro-tubular anode supported solid oxide fuel cells (mT-SOFC) operating at intermediate temperatures (IT) using porous gadolinium-doped ceria (GDC: $Ce_{0.9}Gd_{0.1}O_{2-\delta}$) barrier layers. Rheological studies were performed to determine the deposition conditions by dip coating of the GDC and cathode layers. Two cell configurations (anode/electrolyte/barrier layer/cathode): single-layer cathode (Ni-YSZ/YSZ/GDC/LSCF) and double-layer cathode (Ni-YSZ/YSZ/GDC/LSCF-GDC/LSCF) were fabricated (YSZ: $Zr_{0.92}Y_{0.16}O_{2.08}$; LSCF: $La_{0.6}Sr_{0.4}Co_{0.2}Fe_{0.8}O_{3-\delta}$). Effect of sintering conditions and microstructure features for the GDC layer and cathode layer in cell performance was studied. Current density-voltage (*j-V*) curves and impedance spectroscopy measurements were performed between 650-800 °C, using wet H_2 as fuel and air as oxidant. The double-cathode cells using a GDC layer sintered at 1400 °C with porosity about 50% and pores and grain sizes about 1 μm, showed the best electrochemical response, achieving maximum power densities of up to 160 mW cm^{-2} at 650 °C and about 700 mW cm^{-2} at 800 °C. In this case GDC electrical bridges between cathode and electrolyte are preserved free of insulating phases. A preliminary test under operation at 800 °C shows no degradation at least during the first 100 h.

These results demonstrated that these cells could compete with standard IT-SOFC, and the presented fabrication method is applicable for industrial-scale.

Keywords: A. Dip coating; C. Electrochemical properties; D. GDC; E. Fuel cells

---

1. Introduction

Currently there is a special interest in developing micro-tubular solid oxide fuel cells (mT-SOFC) for their use in portable energy systems. A rapid start-up and shut-down, an increase in the volumetric power density, a better thermal shock resistance together with a low thermal mass allows mT-SOFC devices to compete advantageously with other SOFC geometries [1-4]. Furthermore, mechanical robustness and long-term stability of these micro-tubular cells are also an advantage [5, 6]. Therefore, all these features combined with the fact that mT-SOFCs are smaller, lighter, cleaner and even cheaper than lithium batteries [7], makes them stand out as highly attractive technology for transportable devices. Their properties, performance and manufacturing techniques of mT-SOFCs have been recently reviewed [8-12].

The current challenge is to reduce the working temperature of mT-SOFCs from 800 °C down to an intermediate-temperature range of between 500 and 750 °C (IT-SOFC), which would prevent many of the inconveniences associated with operation at high temperatures. Low-temperature operation would allow the use of inexpensive conventional metals for the stack components, the minimisation of thermal degradation and also the deleterious effects of chemical reactions between cell components [7-13]. However, operating at low temperatures has some drawbacks. Firstly, it decreases cell performance due to the increase in the polarization resistance of the electrodes, as well as a decrease in the ionic conductivity of the electrolyte. In order to reduce the operating temperature, traditional YSZ ($Zr_{0.92}Y_{0.16}O_{2.08}$) electrolyte has been proposed to be replaced by alternative solid electrolytes such as doped ceria, which presents higher ionic conductivity [14]. Another alternative is reducing the thickness of the YSZ electrolyte layer. The main advantage YSZ presents, in addition to its good chemical and mechanical stability, is that YSZ is cheaper than any doped ceria, because it is a material more used in industry. Moreover, ceria-based materials display relatively lower open circuit voltage (OCV) due to high electronic conductivity at the reducing atmosphere [12]. Bearing in mind also that YSZ thin layers can be mass produced reliably using relatively cheap ceramic production routes [15-17], it seems reasonable to

continue developing YSZ-based SOFCs for IT applications. From there, its intrinsic resistance increases substantially [16], and the use of hydrocarbon fuels such as propane, methane, diesel or syngas would require a preliminary stage reforming [18].

Secondly, at low temperatures, the increased polarization on the cathode side might decrease cell performance. In order to reduce cathode polarizations, mixed ionic-electronic conductors (MIEC) have been considered as alternative cathode materials [19-21]. In fact, LSCF ($La_{1-x}Sr_xCo_{1-y}Fe_yO_{3-\delta}$) has been regarded as a promising alternative cathode material because it provides higher ionic-electronic conductivity than LSM (Sr-doped $LaMnO_3$), currently being used at high temperatures [22-24]. The properties of these cobalt-ferrites depend on their composition. $La_{0.6}Sr_{0.4}Co_{0.2}Fe_{0.8}O_{3-\delta}$ seems to be the preferred composition as it presents a good compromise between conductivity, catalytic activity, thermal expansion coefficient (TEC) and reactivity with the electrolyte [20, 25, 26]. This composition is also attractive because high Fe-contents yield a lower TEC than Co-rich compositions, this being optimal for the mismatch of YSZ and doped-CeO_2 electrolytes. However, LSCF cathodes show a tendency to react with YSZ electrolytes, forming electronic and ionic resistant phases, such as $La_2Zr_2O_7$ and $SrZrO_3$, at the interface between the cathode and the electrolyte [13, 27]. Therefore, when using LSCF as the cathode, we need to keep this contamination to the minimum level by using a barrier layer between the electrolyte and the cathode.

Gadolinium-doped ceria (GDC) is well known as a catalytic material and a mixed ionic-electronic conductor [28-30]. Therefore, the insertion of a thin layer of doped ceria between the porous cathode and the electrolyte can help to avoid electrode-electrolyte reactivity. Furthermore, it was reported from electrochemical impedance spectroscopy (EIS) studies that the presence of GDC in the cathode improves oxygen diffusion rates and charge transfers of oxygen ions at the cathode/electrolyte interface, thereby decreasing cathode polarization resistance [31]. Thus, the optimization of cathode composition and microstructure by adding GDC-via ceramic processing routes could help to improve cell performance [32, 33].

However, a critical problem of GDC arises from its poor sinterability. Ceria is highly refractory and exhibits a high melting point (2300 °C), which reduces densification kinetics even at temperatures as high as 1600 °C. As a result, most GDC layers presented in the literature are porous [34-39]. Usually, two alternatives are considered to improve densification. First of all, the use of nanopowders presents the

difficulty of a higher tendency to grain agglomeration and hence to lower densities and sintering defects [37, 38]. Secondly, the use of sintering aids, for example the use of a small amount of Co doping strongly promotes the grain boundary mobility of GDC and enhances the densification rate. However, the excess of cobalt in the GBs (grain boundaries) increases ohmic resistance, reducing the electrochemical performance of SOFCs [40, 41]. Furthermore, although most efforts are focused on to deposit a dense layer of GDC, this results in an increase of the thickness of the electrolyte, and as a consequence of the ohmic resistance of the device. It is also important to keep in mind the stability problems of adhesion between the porous cathode and the electrolyte. Therefore, the study of the behaviour of cells with a porous thin GDC barrier layer, minimizing chemical reactivity with both electrolyte and cathode, will be interesting.

Consequently, the aim of this work is to study the processing parameters to develop porous GDC electrolyte-cathode interlayers produced by conventional ceramic processes. For this purpose, we have to search for a balance between a high sintering of the GDC layer, and minimum cation diffusion from the cathode to the electrolyte. This will make it possible to achieve homogeneous, thin layers with controlled thickness and porosity. We will also investigate the effect of using LSCF-GDC composite cathodes compared with a single LSCF cathode layer. The manufacturing procedures used in this work are fully applicable at an industrial scale, as we are currently fabricating anode supports for mT-SOFC by the extrusion technique [4, 12, 42].

We have fabricated several anode-supported mT-SOFC cells with the following configurations: porous Ni-YSZ anode support, a thin dense YSZ electrolyte layer, a porous thin GDC barrier layer, and a porous LSCF or LSCF-GDC composite cathode. The cathode and the GDC barrier layer were deposited via dip-coating, whereas the electrolyte deposition was performed by wet powder spraying (WPS). Rheological studies have been also performed to determine the deposition conditions of each cell component. The sintering temperature of the GDC layer was varied between 1200 and 1450 °C. Microstructure studies on the cell components and energy dispersive X-ray spectroscopy (EDS) on barrier layer/electrolyte interface were carried out. Finally, the electrochemical characterization of the different cells performed at temperatures between 650 and 800 °C will also be discussed.

2. Experimental

Commercial NiO (Hart Materials, d_{50} = 0.6 μm) and YSZ (TZ-8YS, Tosoh, d_{50} = 0.5 μm) were employed for the anode; YSZ (TZ-8Y, Tosoh, d_{50} = 0.2 μm) for the electrolyte; and $Ce_{0.9}Gd_{0.1}O_{2-\delta}$ (Fuel Cells Materials, d_{50} = 1.0 μm) and $La_{0.6}Sr_{0.4}Co_{0.2}Fe_{0.8}O_{3-\delta}$ (Fuel Cells Materials, d_{50} = 0.3-0.6 μm) powders were employed for the cathode of the cell. The same GDC powders were used for the barrier layers. The impurity level is below the detection limit (~2%) of X-ray diffraction experiments (Rigaku, DMAX-II, Cu Kα).

2.1. Micro-tubular cells fabrication

Microstructural studies limited the optimum fabrication conditions to cells with GDC interlayer sintered at 1300 or 1400 °C. The effect of using a single or double-cathode layer was also studied. Consequently, we will focus on four different types of anode-supported mT-SOFC cells (anode/electrolyte/barrier layer/cathode):

- SC_1300: Ni-YSZ/YSZ/GDC/LSCF (Single cathode, GDC interlayer sintered at 1300 °C)
- SC_1400: Ni-YSZ/YSZ/GDC/LSCF (Single cathode, GDC interlayer sintered at 1400 °C)
- DC_1300: Ni-YSZ/YSZ/GDC/LSCF-GDC/LSCF (Double cathode, GDC interlayer sintered at 1300 °C)
- DC_1400: Ni-YSZ/YSZ/GDC/LSCF-GDC/LSCF (Double cathode, GDC interlayer sintered at 1400 °C)

Table 1 shows the cell fabrication stages.

The supporting ceramic tubes were prepared by cold isostatic pressing (CIP) for 3 min at 200 MPa of previously conditioned NiO-YSZ powders and corn starch pore former with a volume ratio of 50:50, following the procedure outlined in reference 43. The green support tubes were pre-sintered in air by heating them up to 950 °C. YSZ powders were then deposited on anode supports by WPS. The deposited thin electrolyte layer was dried in air at room temperature (RT). Details about powder conditioning using attrition milling to avoid agglomerates formation, as well as slurry preparation, can be found in references [43, 44]. Both anode and electrolyte are cosintered at 1400 °C in air. Optimal sintering conditions have been previously established by dilatometry studies [44]. After sintering, the typical diameter of the tubular cell was 3.5 mm external and 2.6 mm internal, and the length about 120

mm. The electrolyte thickness ranged between 15-20 μm and the area of LSCF cathode was 1 cm^2. The remaining cell components were deposited using dip-coating techniques.

2.2. Optimization of slurries for cathode and barrier layer deposition

Based on previous experience on the study of colloid stability [39], rheological studies have been carried out in order to determine the deposition conditions for the barrier and cathode layers. Rheological properties were studied using a rheometer (*Haake Mars*, rotors DC60/1°, of *Thermo Scientific*, Germany) operating at controlled shear rate (CR) conditions. CR was used to measure the flow curves using a three-stage measuring programme with a linear increase of shear rate from 0 to 1000 s^{-1} in 360 s, a plateau at 1000 s^{-1} for 30 s, and a decrease to zero shear rate in another 360 s. The measurements were performed using a double cone and plate system, with a solvent trap, at a constant temperature of 25 °C. An ultrasonic probe (UP 400S Hielscher Ultrasonics GmbH, Germany) was used to reduce the size of agglomerates.

The suspensions for dip-coating (9–20 vol.% solids) were prepared by mixing the GDC, LSCF or LSCF-GDC powders with an appropriate amount of solvent (ethanol), binder (polyvinyl butyral) and dispersant (phosphate ester). The slurries for GDC interlayer and LSCF or LSCF-GDC cathodes were deposited by dip-coating at a pulling rate within the range of 1.5-4.5 mm s^{-1} to control the coating thickness. The coated films were dried and sintered in air at the temperatures described in Table 1.

2.3. Cells characterization

The microstructure of the cell components was studied in polished transverse cross-sections using secondary and back-scattered electrons images obtained in a field-emission scanning electron microscopy (Merlin FE-SEM, Carl Zeiss, Germany). Both conventional (Everhart-Thornley for secondary electrons) and in-lens detectors (for secondary and backscattered electrons) were used. The microscope was fitted with an energy dispersive analytical system (EDS) for elemental X-ray analysis (INCA450, Oxford Instruments, UK). Resolution of the spatially resolved EDS analysis was estimated by Monte Carlo simulation of electron trajectory in these solids by means of the *Casino v2.48 Software* (University of Sherbrooke, Canada, 2011 [45]).

Current density-voltage and EIS measurements were used for the electrochemical characterization of the cells. The cells were tested using a four-probe set-up with a Ni-foam current collector at the anode side and silver paste at the cathode side. Ag wires were used for the current leads. For the test under operation, gold paste and wires were used at the cathode side (see Figure 1). All cells were characterized at 650, 700, 750 and 800 °C under humidified pure hydrogen atmosphere, using a potentiostat/galvanostat (VSP) fitted with a frequency response analyser (Princeton Applied Research, Oak Ridge, USA). EIS was performed at OCV before and after all potentiodynamic experiments using a sinusoidal signal amplitude of 50 mV over the frequency range of 500 kHz to 0.1 Hz. EIS at OCV was also analysed using the equivalent circuit composed of $LR_{ohm}(R_1Q_1)(R_2Q_2)(R_3Q_3)$ where R_{ohm} represents pure ohmic resistance. Each of the parallel circuits of resistance R and constant phase element Q accounts for its respective depressed semicircle, going from high to low frequencies. A parasitic inductance L was added to account for equipment contribution.

3. Results and discussion

3.1. Optimization of slurries for cathode and barrier layer

The absence of impurity phases in the starting powders was corroborated by XRD experiments. In addition, Li *et al.* reported that there is no chemical reaction between $La_{0.58}Sr_{0.4}Co_{0.2}Fe_{0.8}O_{3-\delta}$ and $Ce_{0.8}Gd_{0.2}O_2$ up to a sintering temperature of 1200 °C [46]. This is probably approximately the maximum sintering temperature of LSCF-GDC based cathodes.

Following the conclusions outlined in a previous study on the stability of GDC colloids, [39] a more detailed study of GDC, LSCF and LSCF-GDC suspensions was carried out. The suspensions were developed using ethanol as the solvent. For this study, we have considered in detail the most important processing parameters for coating fabrication that include solid load, binder concentration and sintering temperature. Rheological studies were performed in order to determine the suspension properties. The aim of these studies was to obtain slurries with sufficiently small particle size and, at the same time, optimum viscosity for successful dip-coating deposition on sintered YSZ electrolytes. A compromise between particle size and viscosity must be reached, which ideally will be for the highest viscosity values just before the suspension reaches the Newtonian fluid behaviour. For this purpose, first agglomerate sizes and then the slurry viscosity were decreased by exposure to ultrasonic probe treatment. The time of

ultrasonic probe treatment is quite critical, as these treatments induce further particle agglomeration. Subsequently, some binder amounts were added to increase the viscosity. In Figure 2, the variation of the viscosity curve with an ultrasonic treatment time of a GDC slurry with 13.0 vol% of solid load and 2.0 wt% of deflocculant is shown. In this case, the optimum viscosity was reached after 3 minutes of ultrasonic treatment followed by the addition of 2.5 wt% of binder, as is also shown in the figure.

Similar studies were carried out for the LSCF and LSCF-GDC 50 wt% suspensions to obtain optimum viscosity values.

As a result, optimum suspensions for the dip-coating process were obtained with 13.0 vol% of solid load, 2.0 wt% of deflocculant, 3 min of ultrasounds and 2.5 wt% of binder, for GDC barrier layer; and 15.0 vol% of solid load, 1 wt% of deflocculant, 1 min of ultrasounds and 2.5 wt% of binder, both for LSCF and LSCF-GDC layers.

After achieving optimum viscosities, GDC and cathode layers were deposited on NiO-YSZ/YSZ co-sintered tubes by dip-coating. FE-SEM studies of transverse sections were performed to determine the layer depth and the optimum sintering temperature for each layer. GDC layers of about 2-4 μm in thickness were deposited with only one dip. 4 or 5 dips were necessary to obtain cathode layers of 20-40 μm in thickness.

In principle, higher sintering temperatures mean better layer adhesion but also lower porosity and possibly more migration of foreign cations into the layers. Since the YSZ-GDC solid solution is known to have a lower conductivity than YSZ and GDC [24, 47, 48], ceria contamination of YSZ electrolyte should be avoided. Therefore, to study the effect of sintering temperature in the quality of interfaces and layer composition, equally deposited GDC barrier layers were sintered at 1300 and 1400 °C, and the interfaces and distribution of cations studied by SEM-EDS analysis. The obtained results are shown in Figure 3 together with the Monte Carlo simulation of electron trajectory in these solids. Simulation results shown that the analysed sample volume is similar in both compounds and in any case it is small as compared with the expected diffusion range of cations. Monte Carlo simulation results guarantee that the EDS microanalytical measurements are suitable to study the cation distribution at the interfaces with a spatial resolution of about 0.5 μm.

3.2. Microstructural characterization

In Figures 4 (a) and (b), we show SEM images obtained by mixing (50%) the secondary and backscattered in-lens signals (acceleration voltage: 0.5 kV, working distance: 2.0 mm) of polished cross-sections of two SC_1300 and SC_1400 cells after electrochemical studies, respectively. The microstructure of electrolyte/barrier layer/cathode and their interfaces is clearly shown. The microstructure features of the anode support and the anode-electrolyte interface in this type of cells have been described previously [44]. The electrolyte is nearly fully dense and only presents a small amount of insignificant closed pores. The estimated electrolyte thickness of the different cells is: 28.1 ± 1.5 μm for SC_1300, 20.8 ± 3.3 μm for DC_1300, 26.9 ± 2.2 μm for SC_1400, and 23.6 ± 4.2 μm for DC_1400. The GDC barrier layer is continuous throughout the electrolyte-cathode interface, presenting a thickness of 2-4 μm and good integration with the electrolyte and the cathode. The GDC layer is porous, with pores connecting the electrolyte directly with the cathode, but also with GDC connecting bridges between the electrolyte and cathode. However, differences between the microstructure of both cells are evident. In the SC_1300 sample, the porosity is higher and the grains of GDC smaller. We performed a study of porosity and grain size of the GDC layers, by image analysis using the *DigitalMicrograph v3.10.0* (Gatan Inc., USA) software. Porosity was determined by image thresholding, whereas the interception method using lines parallel to the interface was used to obtain the grain size. The GDC layer of sample SC_1300 showed a porosity of 63% and an average grain size of 0.7 ± 0.6 μm. Sample SC_1400 showed a porosity of 53% and an average grain size of 1.2 ± 0.9 μm. As expected, there was an increase of GDC grain size and porosity reduction with the increase in sintering temperature. In the latter case, GDC grain size was similar to layer thickness and a connection between electrolyte and cathode through GDC bridges was established.

The compositional EDS maps shown in figures 4 (c) and (d) and the secondary electron images of figures 4 (e) and (f) reveal Sr diffusion from the cathode to the electrolyte surface in both cells, possibly forming small amounts of $SrZrO_3$ phases. A slight reduction of the Sr-Zr phase for the GDC sintered at 1400 °C is shown. The presence of the electrical insulator strontium zirconate phase in the electrolyte-cathode interface may increase the ohmic resistance of the cells, deteriorating their electrochemical performance. However, our results show that Sr diffusion through the GDC phase was inhibited and, consequently, it should take place through the open pores of the GDC barrier. Previous studies prove that the porosity of the GDC layer permits such diffusion [24, 49, 50]. Moreover, a recent

study shows that the diffusion of Sr through cracks in dense-GDC takes place by surface diffusion [51], so we can think that this is the diffusion path through the porous GDC layer. Consequently, $SrZrO_3$ phases are produced at the YSZ-pore interface and they are more abundant, forming a quasi-continuous layer in the case of the GDC barrier sintered at the lowest temperature. However, it is important to note that in the case of the high temperature sintered barrier, a good electrical connection takes place through the wide GDC bridges between electrolyte and cathode.

3.3. Electrochemical characterization

Voltage versus current density (*j-V*) curves were measured at 650, 700, 750 and 800 °C using pure hydrogen humidified with a bubbler at RT (~3% H_2O) as fuel gas for the anode (0.08 L min^{-1}) and static air for the cathode. Voltage and power density versus current density curves for the DC_1400 tubular cell are given in Figure 5. The *j-V* parameters for the four studied cells are presented in Table 2. In all cases, the OCV values are in strong agreement with those predicted by the Nernst equation. This is a sign of a good separation between fuel and oxygen cell chambers, the consequence of proper tube sealing and the tightness of the YSZ electrolyte layer. There is only one deviation from the Nernst prediction (cell DC_1300 at 650 °C), which is also consistent with the noise observed in the *j-V* experiments for these conditions. The reason for this effect is probably a slight deterioration of the sealing, producing a small gas leakage, as this was the last experiment performed in this cell after several heating and cooling cycles.

For all the cells, the electrochemical performance increased when increasing the operation temperature, as expected. It is evident that an increase in the sintering temperature of the GDC interlayer leads to an improvement in cell performance: for example, power density for SC_x cells increases by 35% at 650 °C and by 29% at 800 °C. For DC_x samples, that increase is 33% at 650 °C and 30% at 800 °C. This is clearly due to the differences in microstructure between the layers. In the case of SC_1400 samples, the GDC grain size is similar to layer thickness and a good connection between electrolyte and cathode through GDC bridges is established. GDC is an excellent catalyser of oxygen reduction reactions taking place at the cathode side. The role of GDC in increasing cathode reaction rates is further evidenced when comparing the performance of single and double-cathode layers. In fact, replacing the LSCF single-cathode SC_x samples with the LSCF-GDC/LSCF double-cathode DC_x samples produces an increase in power density that is more noticeable at low operation temperatures (see Table 2). The latter confirms

that the addition of GDC to the LSCF cathode decreases its polarization resistance [31]. Furthermore, if we compare the power output results with those of similar cells fabricated in our laboratories, but with LSM cathodes and LSM-YSZ composite cathodes, we can conclude that the replacement of standard LSM with LSCF-based cathodes permits a reduction in the operation temperature of about 100 °C [44, 52].

These results show that, the micro-tubular cells fabricated with porous GDC layer are competitive. Yamaguchi and Sammes [53] have reported a current density of 80 mA cm^{-2} at 750 °C and 0.7 V, on a double-cathode mT-SOFC without GDC barrier layer, fabricated by extrusión and dip-coating. Liu *et al.* [54] obtained a current density of 170 mA cm^{-2} at 800 °C and 0.7 V, on a micro-tubular electrolyte-supported cell, with LSCF single-cathode and also without GDC interlayer. Suzuki *et al.* achieved a better performance using nanometric powders and an electrolyte thickness less than 1 μm. They obtained values of 430 mA cm^{-2} at 600 °C and 0.7 V for a double-cathode micro-cell prepared by dip-coating [55]. In the same way, Sumi *et al.* using nanometric powders and an electrolyte thickness of 5 μm, obtained 1000 mA cm^{-2} in 40%H_2 in N_2 at 700 °C and 0.7 V for a SC_1400 cell [56]. In any case, those cells with nanometric powders do not present much long-term stability [57, 58]. Note that, although most of the high cell outputs reported in the literature correspond to planar designs, the comparison was made only between micro-tubular cells. Finally, H. Fan *et al*. in a recent work [59] have studied a planar SOFC cell using the same components as for the SC_1300 cell, achieving a lower electrochemical performance than our cells.

The DC_1400 cell with the best electrochemical performance was also fabricated using an extruded anode support and tested under operation at 800 °C for 100 h. No degradation or aging effects were observed. This result agrees with the fact that in the DC_1400 cells, the Sr-Zr phases generated during the manufacturing process in the YSZ/cathode interface are discontinuous species that not evolve under operation.

3.4. Electrochemical Impedance Spectroscopy

Electrochemical Impedance Spectroscopy (EIS) experiments were performed under OCV conditions, before and after cell operation, for all the *j-V* measurements. It is noticeable that no variation was observed in any case before and after SOFC operation, assuring no significant degradation of the

cells. EIS results for the DC_1400 cell are shown in Figure 6. A summary of the fitting parameters for all the cells and temperatures is also given in Table 3. The main conclusion is that, according to the Area Specific Resistance (ASR) values, best performance is obtained for the cell with the GDC interlayer sintered at 1400 °C, due to the presence of large GDC grains connecting the cathode to the electrolyte, and with a double-layer LSCF-GDC/LSCF cathode. GDC interlayer sintering temperature improves cell performance at low-temperature operation. The results are clearly in agreement with the *j-V* results discussed above and in connection with the characteristics of interlayer microstructure and the favourable effect of GDC in the cathode polarization. Variations in ohmic resistance (R_{ohm}) values are due to slight changes in electrolyte and interlayer thickness from cell to cell. The cell with the thicker electrolyte (SC_1300) shows the higher R_{ohm}, and the cell with the thinner electrolyte (DC_1300), the lowest R_{ohm}. They are also slightly higher than those expected for a cell without the GDC porous interlayer. For the SC_x configuration, the cell sintered at a lower temperature (SC_1300) showed higher R_{ohm} values than sample SC_1400 (sintered at 1400 °C), as a consequence of the higher porosity of the GDC interlayer. However, for DC_x cells this effect is not observed, as higher R_{ohm} values are obtained for DC_1400 (sintered at 1400 °C). We attribute this increase of R_{ohm} contribution in this cell to lateral conduction losses at the cathode current collector, as the silver wire was not perfectly attached when we concluded that experiment. Despite this increase of the ohmic contribution for this cell, polarization resistance results are consistent when compared with the other cells.

In line with the *j-V* results, EIS analysis also showed lower polarization resistances for cells using LSCF-GDC composite cathodes. In addition, it is very difficult to attribute R_1, R_2 and R_3 components to anode or cathode diffusion or charge transfer contribution, as those processes are generally overlapped. However, it was observed that the R_2 component seems to be almost identical for all the studied cell configurations. For this reason this contribution was tentatively associated with the anode, mainly to diffusion processes through the anode support [42]. Based on previous literature data, R_1 and R_3 contributions can be attributed to cathode diffusion and activation, respectively [31, 60], but no clear dependence on cell morphology can be established. EIS analysis under polarization, the use of reference electrodes, and a comparison with other cathode materials (LSM-YSZ and $Pr_2NiO_{4+\delta}$) are currently under investigation in order to fully resolve all the contributions from the EIS studies.

4. Conclusions

The effect of the cathode morphology and of the GDC interlayer on the performance of Ni–YSZ/YSZ/GDC/LSCF micro-tubular SOFCs has been studied. A double-layer LSCF-GDC/LSCF cathode and high sintering temperature for the GDC barrier layer increases cell performance. Sintering conditions of the GDC interlayer were adjusted at 1400 °C. The interlayer is porous and Sr-Zr phases were detected mainly in the pore/YSZ interface. The electrical insulating Sr-Zr phases originated during electrode sintering, but those species do not evolve under operation. Double-cathode cells with a GDC porous barrier layer sintered at 1400 °C cell show maximum power densities of up to 160 mW cm^{-2} at 650 °C and about 700 mW cm^{-2} at 800 °C. As a summary, this cathode configuration and the excellent integration with the electrolyte permit the successful fabrication of competitive mT-SOFCs using a conventional ceramic procedure, which can be applicable on an industrial scale.

Acknowledgements

This work was supported under the project financed by the Spanish Government and the European Community (FEDER program) MAT2012-30763. The authors wish to thank Dr. Rodrigo Moreno for their advice on rheological studies.

References

[1] W. Bujalski, C.M. Dikwal, K. Kendall, Cycling of three solid oxide fuel cell types, J. Power Sources 171 (2007) 96–100.

[2] Y. Du, N.M. Sammes, Fabrication of tubular electrolytes for solid oxide fuel cells using strontium- and magnesium-doped $LaGaO_3$ materials, J. Eur. Ceram. Soc. 21 (2001) 727–735.

[3] P. Sarkar, L. Yamarte, H. Rho, L. Johanson, Anode-supported tubular micro-solid oxide fuel cell, Int. J. Appl. Ceram. Technol. 4 (2007) 103–108.

[4] K. Kendall, Progress in microtubular solid oxide fuel cells, Int. J. Appl. Ceram. Technol. 7 (2010) 1–9.

[5] J. Van Herle, R. Ihringer, N.M. Sammes, G. Tompsett, K. Kendall, K. Yamada, C. Wen, T. Kawada, M. Ihara, J. Mizusaki, Concept and technology of SOFC for electric vehicles, Solid State Ionics 132 (2000) 333–342.

[6] M.A. Laguna-Bercero, A. Férriz, A. Larrea, L. Correas, V.M. Orera, Long-term stability studies of anode-supported micro-tubular solid oxide fuel cells, Fuel Cells 13 (2013) 1116–1122.

[7] B.C.H. Steele, A. Heinzel, Materials for fuel-cell technologies, Nature 414 (2001) 345–342.

[8] V. Lawlor, S. Griesses, G. Buchinger, A.G. Olabi, S. Cordiner, D. Meissner, Review of the micro-tubular solid oxide fuel cell. Part I. Stack design issues and research activities, J. Power Sources 193 (2009) 387–399.

[9] V. Lawlor, Review of the micro-tubular solid oxide fuel cell (Part II: Cell design issues and research activities), J. Power Sources 240 (2013) 421–441.

[10] V.M. Orera, M.A. Laguna-Bercero, A. Larrea, Fabrication methods and performance in fuel cell and steam electrolysis operation modes of small tubular solid oxide fuel cell (SOFCs): a review, Front Energy Res 2 (2014) 22.

[11] P. Sarkar, S. Amiri, Advances in micro solid oxide fuel cells, in: Jain & Shen (Eds.) Nanostructured and advanced materials for fuel cells, CRC Press, USA, 2013, pp. 69-126.

[12] T. Suzuki, Y. Funahashi, T. Yamaguchi, Y. Fujishiro, M. Awano, Development of fabrication/integration technology for micro tubular SOFCs, in: Micro fuel cells: principles and applications, Elsevier Inc., USA, 2009, pp. 141-177.

[13] N.Q. Minh, Ceramic fuel cells, J. Am. Ceram. Soc. 76-3 (1993) 563–588.

[14] B. Dalslet, P. Blennow, P. Vang Hendriksen, N. Bonanos, D. Lybye, M. Mogensen, Assessment of doped ceria as electrolyte, J. Solid State Electrochem 10 (2006) 547–561.

[15] L.C. De Jonghe, C.P. Jacobson, S.J. Visco, Supported electrolyte thin film synthesis of solid oxide fuel cells, Fuel Cells, Annu Rev Mater Res 33 (2003) 169–182.

[16] J. Peña-Martínez, D. Marrero-López, C. Sánchez-Bautista, A.J. Dos Santos-García, J.C. Ruiz-Morales, J. Canales-Vázquez, P. Núñez, Effect of a CGO buffer layer on the performance of $(La_{0.6}Sr_{0.4})_{0.995}Co_{0.2}Fe_{0.8}O_{3-\delta}$ cathode in YSZ-Based SOFC, Bol. Soc. Esp. Ceram. 49-1 (2010) 15–22.

[17] E. Ivers-Tiffée, A. Weber, D. Herbstritt, Materials and technologies for SOFC-components, J. Eur. Ceram. Soc. 21 (2001) 1805–1811.

[18] J.H. Hirschenhofer, D.B. Stauffer, R.R. Engleman, M.G. Klett, in: Fuel Cell Handbook, 4th Edition, DOE/FETC-99/1076, US Department of Energy, Federal Energy Technology Center, Morgantown (WV), 1998.

[19] Y. Takeda, R. Kanno, M. Noda, Y. Tomida, O. Yamamoto, Cathodic polarization phenomena of perovskite oxide electrodes with stabilized zirconia, J. Electrochem. Soc. 134 (1987) 2656–2661.

[20] L.W. Tai, M.M. Nasrallah, H.U. Anderson, D.M. Sparlin, S.R. Sehlin, Structure and electrical properties of $La_{1-x}Sr_xCo_{1-y}Fe_yO_3$. Part 1. The system $La_{0.8}Sr_{0.2}Co_{1-y}Fe_yO_3$, Solid State Ionics 76 (1995) 259–271.

[21] J.W. Stevenson, T.R. Armstrong, R.D. Carneim, L.R. Pederson, W.J. Weber, Electrochemical properties of mixed conducting perovskites $La_{1-x}M_xCo_{1-y}Fe_yO_{3-\delta}$ (M = Sr, Ba, Ca), J. Electrochem. Soc. 143 (1996) 2722–2729.

[22] S. Sekido, H. Tachibana, Y. Yamamura, T. Kambara, Electric-ionic conductivity in perovskite-type oxides $Sr_xLa_{1-x}Co_{1-y}O_{3-\delta}$, Solid State Ionics 37 (1990) 253–259.

[23] V.A.C. Hannappel, A. Mai, J. Mertens, Electrode activation of anode-supported SOFCs with LSM- and LSCF-type cathodes, Solid State Ionics 177 (2006) 2033–2037.

[24] W.H. Kim, H.S. Song, J. Moon, H.W. Lee, Intermediate temperature solid oxide fuel cell using (La,Sr)(Co,Fe)O_3–based cathodes, Solid State Ionics 177 (2006) 3211–3216.

[25] W.G. Wang, M. Mogensen, High-performance lanthanum-ferrite-based cathode for SOFC, Solid State Ionics 176 (2005) 457–462.

[26] L.W. Tai, M.M. Nasrallah, H.U. Anderson, D.M. Sparlin, S.R. Sehlin, Structure and electrical properties of $La_{1-x}Sr_xCo_{1-y}Fe_yO_3$. Part 2. The system $La_{1-x}Sr_xCo_{0.2}Fe_{0.8}O_3$, Solid State Ionics 76 (1995) 273–283.

[27] H.Y. Lee, W.S. Cho, S.M. Oh, Active reaction sites and oxygen reduction kinetics on $La_{1-x}Sr_xMnO_{3+\delta}$ (x=0.1-0.4)/YSZ (Yttria-Stabilized Zirconia) electrodes for solid oxide fuel cells, Bull. Korean Chem. Soc. 19 (1998) 661–666.

[28] H. Yahiro, K. Eguchi, H. Aria, Electrical properties and reproducibilities of ceria–rare-earth oxide systems and their application to solid oxide fuel cell, Solid State Ionics 36 (1989) 71–75.

[29] D.L. Maricle, T.E. Swarr, S. Karavolis, Enhanced ceria a low-temperature SOFC electrolyte, Solid State Ionics 52 (1992) 173–18.

[30] B.C.H. Steele, Appraisal of $Ce_{1-y}Gd_yO_{2-y/2}$ electrolytes for IT-SOFC operation at 500 °C, Solid State Ionics 129 (2000) 95–110.

[31] V. Dusastre, J.A. Kilner, Optimisation of composite cathodes for intermediate temperature SOFC applications, Solid State Ionics 126 (1999) 163–174.

[32] F. Qiang, K. Sun, N. Zhang, S. Le, X. Zhu, J.H. Piao, Optimization on fabrication and performance of A-site-deficient $La_{0.58}Sr_{0.4}Co_{0.2}Fe_{0.8}O_{3-\delta}$ cathode for SOFC, J. Solid State Electrochem. 13 (2009) 455–467.

[33] S.M. Haile, Fuel cells materials and components, Acta Mater. 51 (2003) 5981–6000.

[34] A. Mai, V.A.C. Haanappel, S. Uhlenbruck, F. Tietz, D. Stöver, Ferrite-based perovskites as cathode materials for anode-supported solid oxide fuel cells, Solid State Ionics 176 (2005) 1341–1350.

[35] S. Uhlenbruck, N. Jordan, D. Sebold, H.P. Buchkremer, V.A.C. Haanappel, D. Stöver, Thin film coating technologies of $(Ce,Gd)O_{2-\delta}$ interlayers for application in ceramic high-temperature fuel cells, Thin Solid Films 515 (2007) 4053–4060.

[36] D.F. Wang, J.X. Wang, C.R. He, Y.K. Tao, C. Xu, W.G. Wang, Preparation of a $Gd_{0.1}Ce_{0.9}O_{2-\delta}$ interlayer for intermediate-temperature solid oxide fuel cells by spray coating, J. Alloys. Compd. 505 (2010) 118–124.

[37] V. Gil, J. Gurauskis, R. Campana, R.I. Merino, A. Larrea, V.M. Orera, Anode-supported micro-tubular cells fabricated with gadolinia-doped ceria nanopowders, J. Power Sources 196 (2011) 1184–1190.

[38] Y. Gong, W. Ji, L. Zhang, M. Li, B. Xie, H. Wang, Y. Jian, Y. Song, Low temperature deposited $(Ce,Gd)O_{2-x}$ interlayer for $La_{0.6}Sr_{0.4}Co_{0.2}Fe_{0.8}O_3$ cathode based solid oxide fuel cell, J. Power Sources 196 (2011) 2768–2772.

[39] M.J. López Robledo, J. Silva Treviño, T. Molina, R. Moreno, Colloidal stability of gadolinium-doped ceria powder in aqueous and non-aqueous media, J. Eur. Ceram. Soc. 33 (2013) 297–303.

[40] C. Kleinlogel, L.J. Gauckler, Sintering and properties of nanosized ceria solid solutions, Solid State Ionics 135 (2000) 567–573.

[41] J.H. Song, M.G. Jung, H.W. Park, H.T. Lim, The effect of fabrication conditions for GDC buffer layer on electrochemical performance of solid oxide fuel cells, Nano-Micro Lett. 5-3 (2013) 151–158.

[42] H. Monzón, M.A. Laguna-Bercero, A. Larrea, B.I. Arias, A. Várez, B. Levenfeld, Design of industrially scalable microtubular solid oxide fuel cells based on an extruded support, J. Hydrogen Energy 39-10 (2014) 5470–5476.

[43] R. Campana, A. Larrea, R.I. Merino, I. Villarreal, V.M. Orera, SOFC mini-tubulares basadas en YSZ, Bol. Soc. Esp. Ceram. 47 (2008) 189–195.

[44] [43] R. Campana, A. Larrea, R.I. Merino, I. Villarreal, V.M. Orera, Fabrication, electrochemical characterization and thermal cycling of anode supported micro-tubular solid oxide fuel cells, J. Power Sources 192 (2009) 120–125.

[45] P. Hovington, D. Drouin, R. Gauvin, CASINO: a new era of Monte Carlo code in C language for the electron beam interaction - Part I: description of the program, Scanning 19 (1997) 1–14.

[46] N. Li, A. Verma, P. Singh, J.H. Kim, Characterization of $La_{0.58}Sr_{0.4}Co_{0.2}Fe_{0.8}O_{3-\delta}$–$Ce_{0.8}Gd_{0.2}O_2$ composite cathode for intermediate temperature solid oxide fuel cells, Ceramics International 39 (2013) 529–538.

[47] A. Tsoga, A. Gupta, A. Naoumidis, P. Nikolopoulos, Gadolinia-doped ceria and yttria stabilized zirconia interfaces: regarding their application for SOFC technology, Acta Mater 48 (2000) 4709–4714.

[48] X.D. Zhou, B. Scarfino, H.U. Anderson, Electrical conductivity and stability of Gd-doped ceria/Y-doped zirconia ceramics and thin films, Solid State Ionics 175 (2004) 19–22.

[49] J.W. Yun, J. Han, S.P. Yoon, S. Park, Y.S. Kim, S.W. Nam, $Ce_{0.8}Gd_{0.2}O_2$ modification on $La_{0.6}Sr_{0.4}Co_{0.2}Fe_{0.8}O_3$ cathode for improving a cell performance in intermediate temperature solid oxide fuel cells, J. Ind. Eng. Chem. 17 (2011) 439–444.

[50] Y.C.H. Chang, M.C.H. Lee, W.X. Kao, C.H.H. Wang, T.N. Lin, J.C.H. Chang, Fabrication and evaluation of electrochemical characteristics of the composite cathode layers for the anode-supported solid-oxide fuel cells, J. Taiwan Inst. Chem. E 42 (2011) 775–782.

[51] F. Wang, M. Nishi, M.E. Brito, H. Kishimoto, K. Yamaji, H. Yokokawa, T. Horita, Sr and Zr diffusion in LSCF/10GDC/8YSZ triplets for solid oxide fuel cells (SOFCs), J. Power Sources 258 (2014) 281–289.

[52] M.A. Laguna-Bercero, R. Campana, A. Larrea, J.A. Kilner, V.M. Orera, Performance and aging of micro-tubular YSZ-based solid oxide regenerative fuel cells, Fuel Cells 11 (2011) 116–123.

[53] T. Yamaguchi, N. Sammes, Electrochemical performances of a thin film type SOFC on a porous micro-tubular support, ECS Transactions 33-40 (2011) 143–148.

[54] Y. Liu, N. Liu, X.Y. Tan, Preparation of microtubular solid oxide fuel cells based on highly asymmetric structured electrolyte hollow fibers, Sci. China Chem. 54-5 (2011) 850–855.

[55] T. Suzuki, Md.H. Zahir, T. Yamaguchi, Y. Fujishiro, N. Sammes, Fabrication of micro-tubular solid oxide fuel cells with a single-grain-thick yttria stabilized zirconia electrolyte, J. Power Sources 195 (2010) 7825–7828.

[56] H. Sumi, T. Yamaguchi, K. Hamamoto, T. Suzuki, Y. Fujishiro, T. Matsui, K. Eguchi, AC impedance characteristics for anode-supported micro-tubular solid oxide fuel cells, Electrochim. Acta 67 (2012) 159–165.

[57] M. Shah, P.W. Voorhees, S.A. Barnett, Time-dependent performance changes in LSCF-infiltrated SOFC cathodes: the role of nano-particle coarsening, Solid State Ionics 187 (2011) 64–67.

[58] Y. Liu, F. Wang, B. Chi, J. Pu, L. Jian, S.P. Jiang, A stability study of impregnated LSCF–GDC composite cathodes of solid oxide fuel cells, J. Alloys Compd. 578 (2013) 37–43.

[59] H. Fan, M. Keane, P. Singh, M. Han, Electrochemical performance and stability of lanthanum strontium cobalt ferrite oxygen electrode with gadolinia doped ceria barrier layer for reversible solid oxide fuel cell, J. Power Sources 268 (2014) 634–639.

[60] E. Perry Murray, M.J. Sever, S.A. Barnett, Electrochemical performance of $(La,Sr)(Co,Fe)O_3$–$(Ce,Gd)O_3$ composite cathodes, Solid State Ionics 148 (2002) 27–34.

FIGURE CAPTIONS

Fig. 1 Photograph of a cell showing current collection leads and how the 4-probe connections are made

Fig. 2 Viscosity curves of GDC in ethanol with 13.0 vol% solid load, 2.0 wt% of deflocculant and exposed to 1, 2, 3, 4, 5 and 6 minutes of ultrasonic probe treatment. Results for the slurry homogenized during 3 min. plus 2.5 wt% of binder are also shown

Fig. 3 Top: Monte Carlo simulation of electron trajectories on GDC and YSZ layers. Bottom: variation of the [Ce] atomic fraction, expressed as [Ce]/([Ce]+[Zr]) atomic ratio, across the GDC/YSZ interface, for GDC layers sintered at 1300 °C and 1400 °C. The atomic concentrations were obtained from EDS quantitative microanalysis

Fig. 4 SEM images of cross-sections of micro-tubular cells SC_1300 (a, c and e), and SC_1400 (b, d and f), after being operated for electrochemical test. The high porosity of the GDC layer is shown. Images (a) and (b) were obtained by mixing (50%) the signals from the secondary and backscattered in-lens detectors.
In (c) and (d) compositional EDS maps of Sr (red), Ce (green) and Zr (blue) are showed (acceleration voltage: 14.0 kV, probe current: 600 pA, map resolution: 256x256, map dwell: 500 µs, frames: 10). Lanthanum map is not shown for reasons of clarity, as it does not diffuse into the electrolyte. In (e) and (f) the arrow indicates the Sr-Zr insulating phase formed during fabrication process. Images (e) and (f) were obtained using the Everhart-Thornley secondary electron detector

Fig. 5 Voltage (left axis) and power density (right axis) versus current density curves for the DC_1400 microtubular cell, measured at 650, 700, 750 and 800 °C

Fig. 6 EIS results for the DC_1400 cell at different temperatures

Figure 1

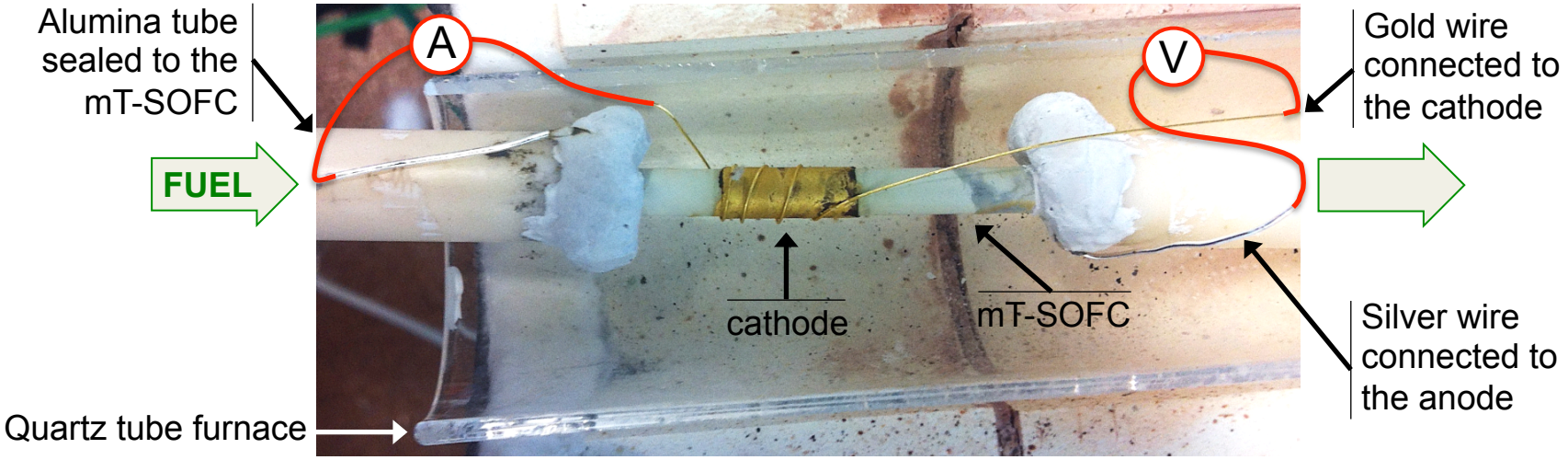
Alumina tube sealed to the mT-SOFC
FUEL
A
V
Gold wire connected to the cathode
cathode
mT-SOFC
Silver wire connected to the anode
Quartz tube furnace

Figure 2

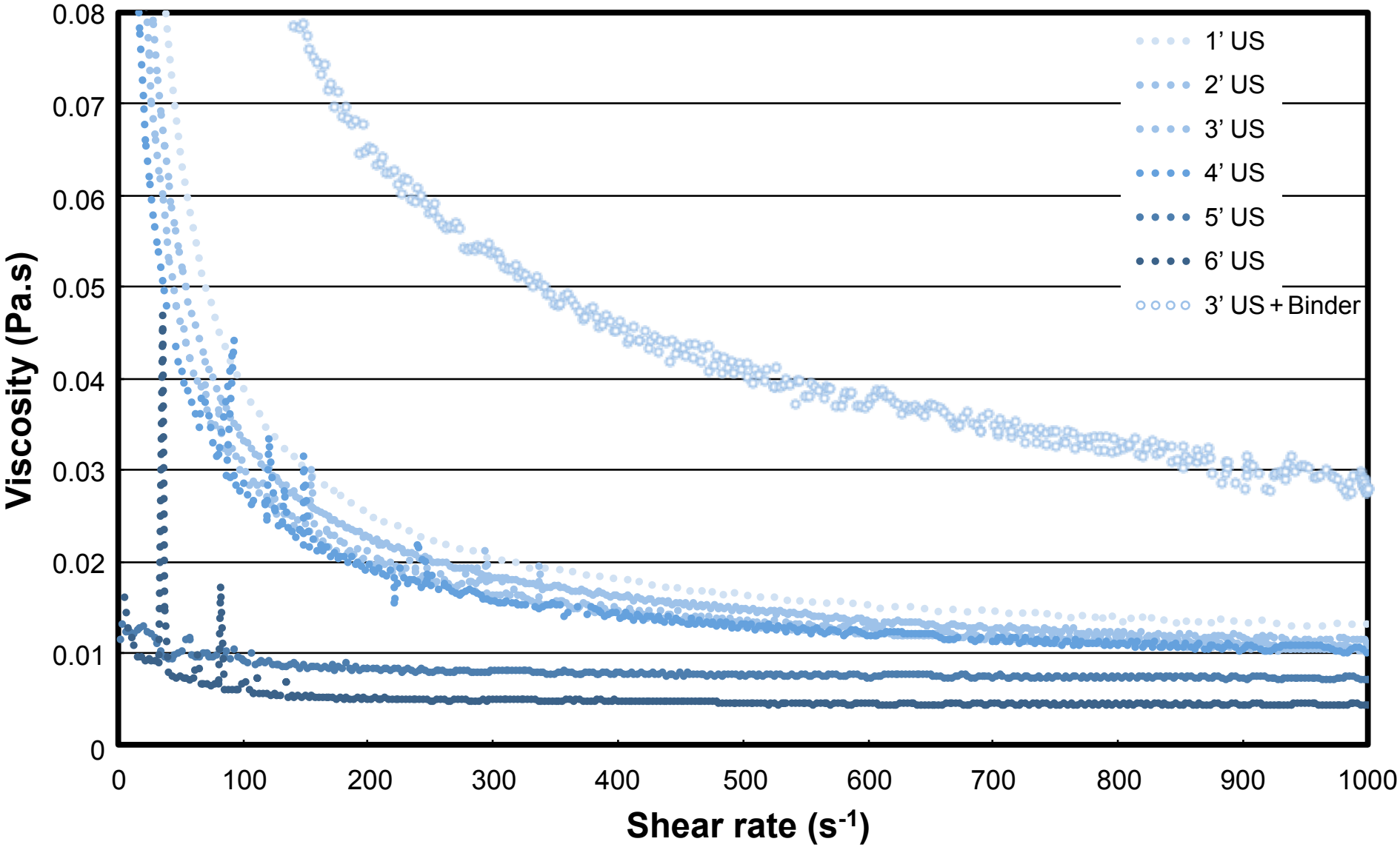
0.08
0.07
0.06
0.05
0.04
0.03
0.02
0.01
0
Viscosity (Pa.s)
0
100
200
300
400
500
600
700
800
900
1000
Shear rate (s-1)
1' US
2' US
3' US
4' US
5' US
6' US
3' US + Binder

Figure 3

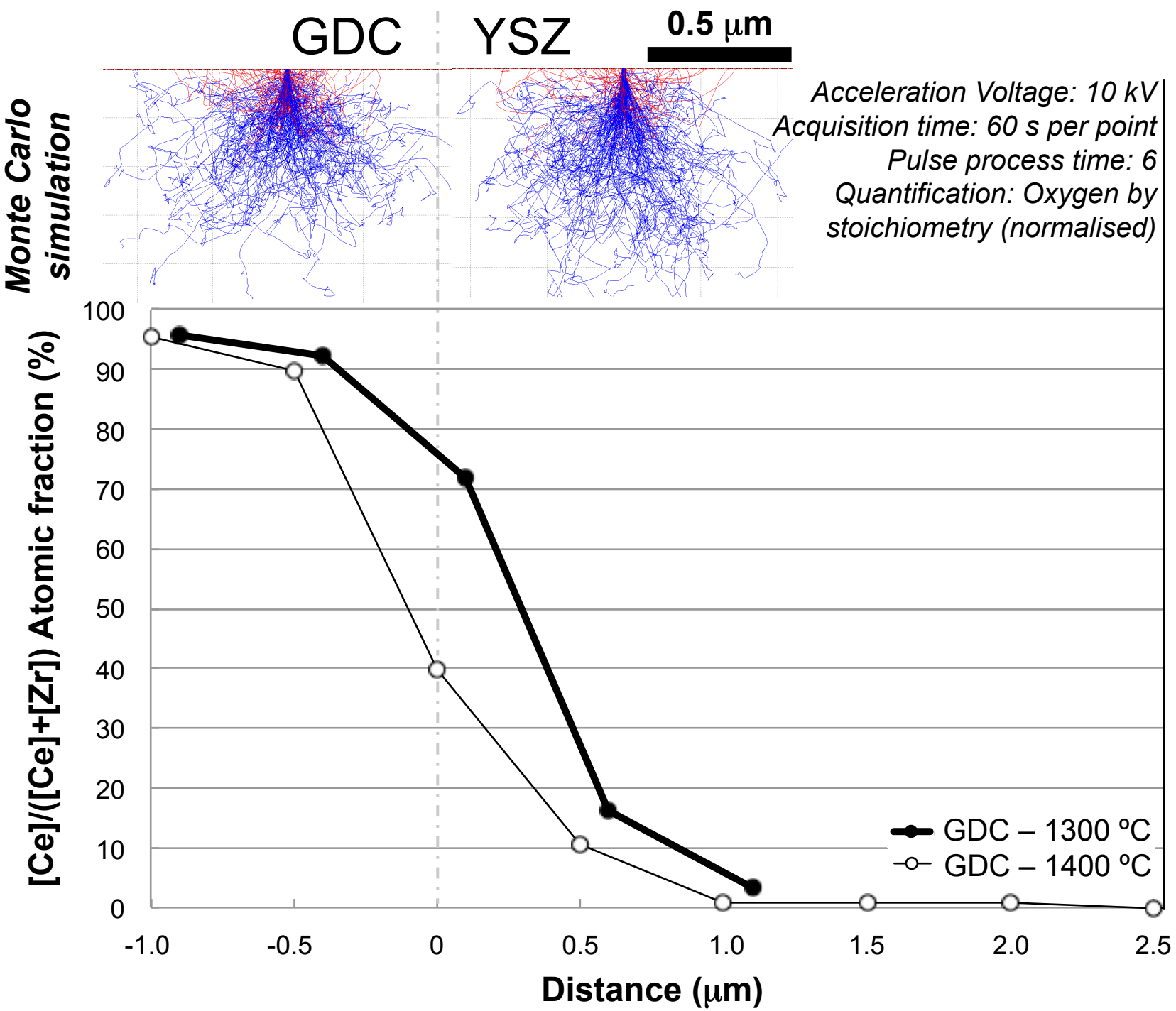
GDC
YSZ
0.5 μm
Monte Carlo simulation
Acceleration Voltage: 10 kV
Acquisition time: 60 s per point
Pulse process time: 6
Quantification: Oxygen by stoichiometry (normalised)
[Ce]/([Ce]+[Zr]) Atomic fraction (%)
100
90
80
70
60
50
40
30
20
10
0
-1.0
-0.5
0
0.5
1.0
1.5
2.0
2.5
Distance (μm)
GDC – 1300 ºC
GDC – 1400 ºC

Figure 4

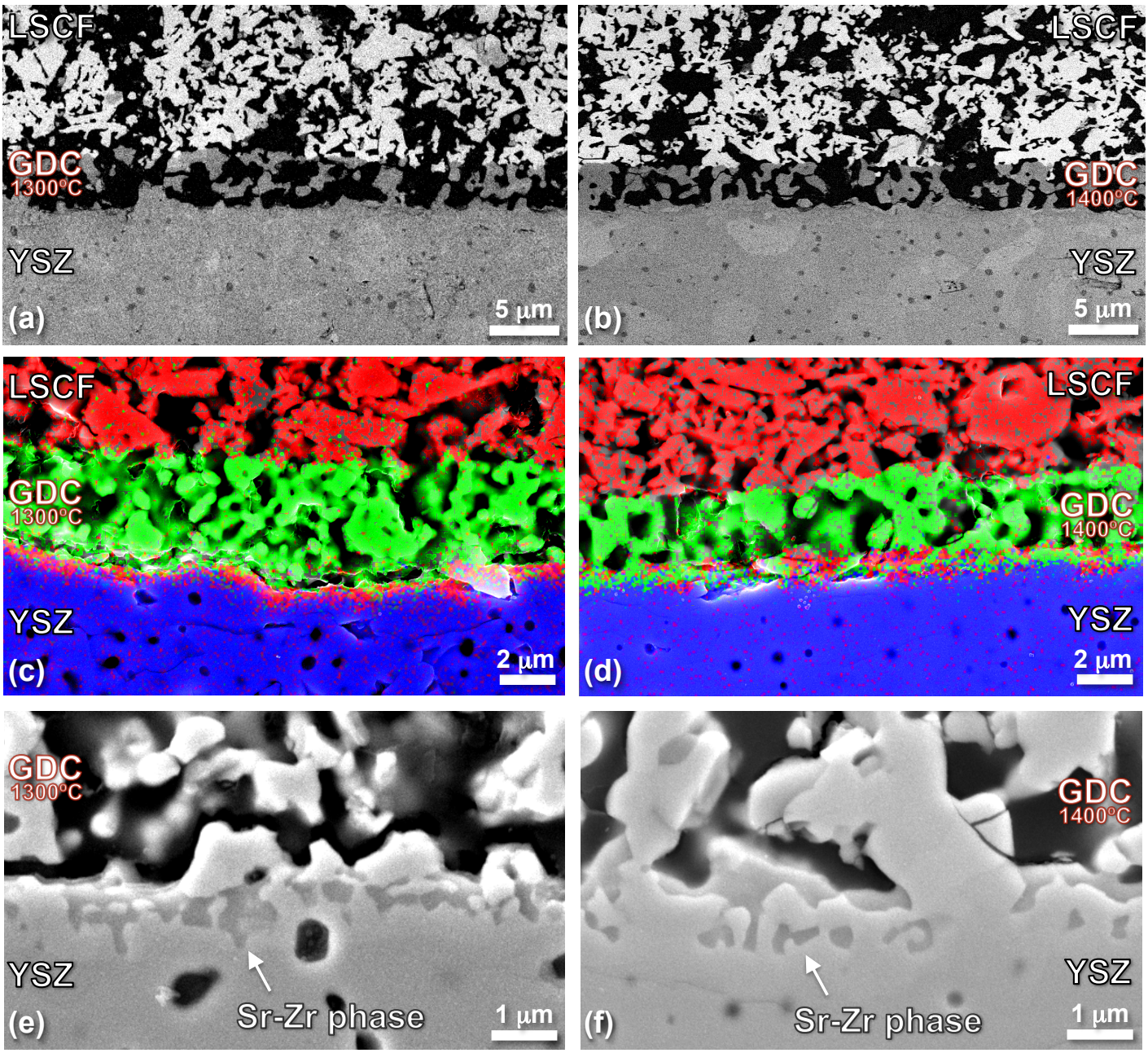
LSCF
GDC
1300°C
YSZ
(a)
5 μm
LSCF
GDC
1400°C
YSZ
(b)
5 μm
LSCF
GDC
1300°C
YSZ
(c)
2 μm
LSCF
GDC
1400°C
YSZ
(d)
2 μm
GDC
1300°C
YSZ
Sr-Zr phase
(e)
1 μm
GDC
1400°C
YSZ
Sr-Zr phase
(f)
1 μm

Figure 5

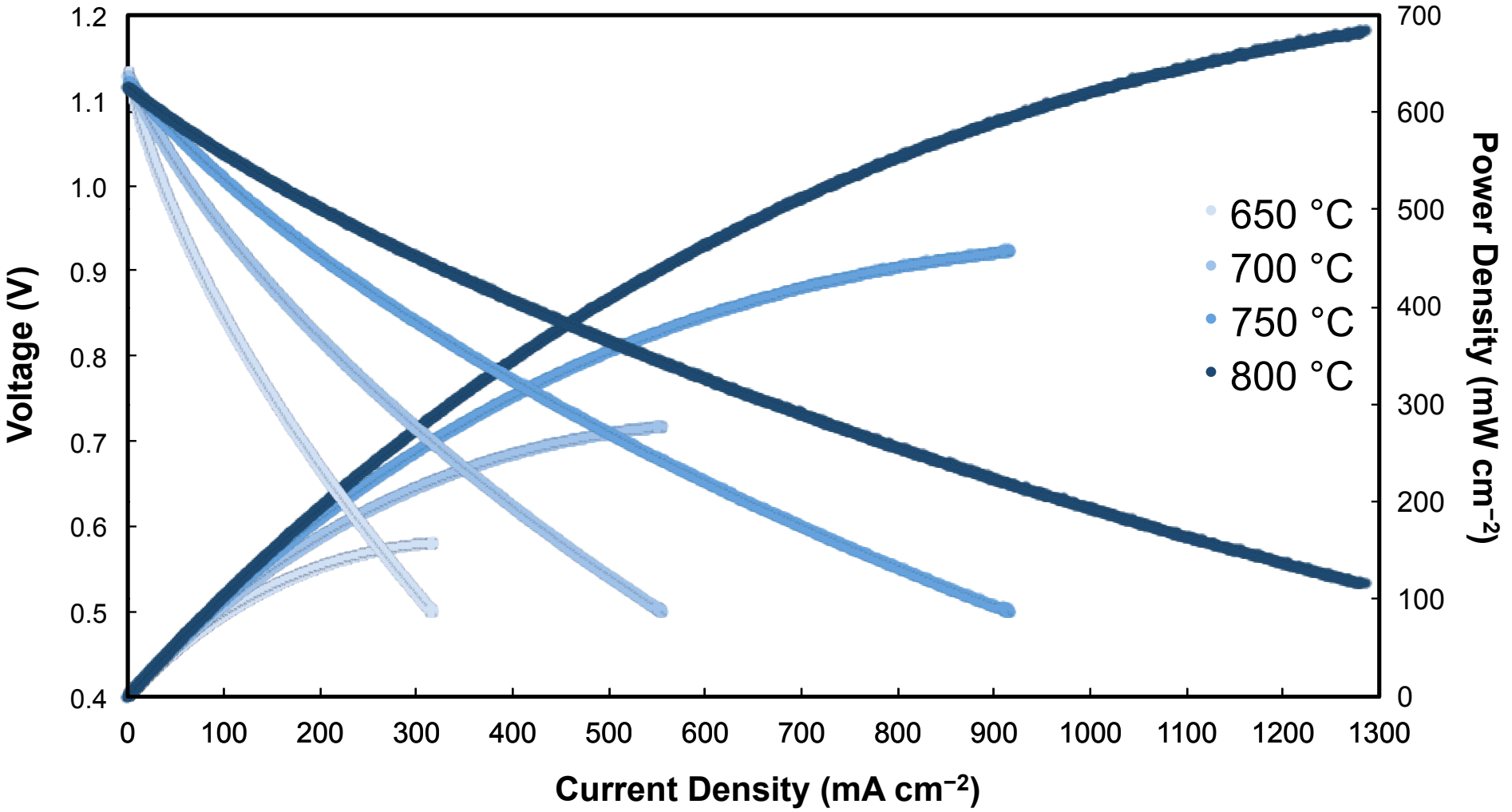
Voltage (V)
1.2
1.1
1.0
0.9
0.8
0.7
0.6
0.5
0.4
Power Density (mW cm⁻²)
700
600
500
400
300
200
100
0
0
100
200
300
400
500
600
700
800
900
1000
1100
1200
1300
Current Density (mA cm⁻²)
650 °C
700 °C
750 °C
800 °C

Figure 6

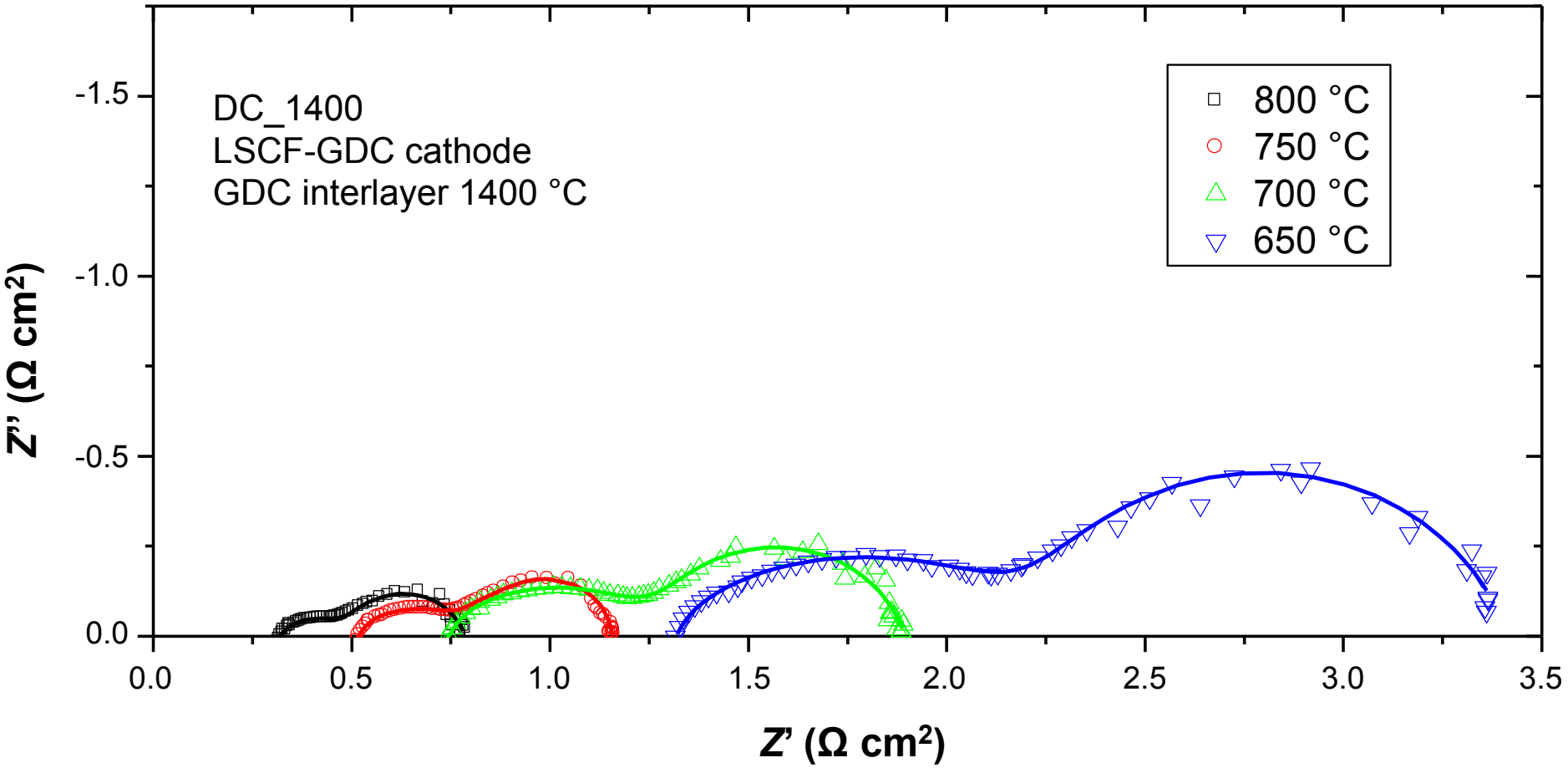
DC_1400
LSCF-GDC cathode
GDC interlayer 1400 °C
800 °C
750 °C
700 °C
650 °C
-1.5
-1.0
-0.5
0.0
0.0
0.5
1.0
1.5
2.0
2.5
3.0
3.5
Z’’ (Ω cm²)
Z’ (Ω cm²)

TABLES

Microtubular cell fabrication steps[a]	Details / Method
Anode	
1. NiO-YSZ support[b]	(1) Cold isostatic pressing (2) Pre-sintering (950 °C, 4 h) - Thickness ~ 400 µm
Electrolyte	
2. YSZ	(1) Wet powder spraying (2) Sintering (1400 °C, 2 h) - Thickness ~ 20 µm
Barrier layer	
3. GDC	(1) Dip-coating (2) Sintering (1300 or 1400 °C, 2 h) - Thickness ~ 3 µm
Cathode	
4. LSCF	(1) Dip-coating (2) Sintering (1150 °C, 2 h) - Thickness ~ 40 µm
5. LSCF-GDC/LSCF[c]	(1) LSCF-GDC dip-coating (2) Sintering (1150 °C, 2h) - Thickness ~ 30 µm (3) LSCF dip-coating (4) Sintering (1150 °C, 2h) - Thickness ~ 30 µm

Table 1. Summary of the various steps involved in micro-tubular cell fabrication

[a] Steps for Micro-tubular cell 1: 1 → 2 → 3 → 4; Micro-tubular cell 2: 1 → 2 → 3 → 5.
[b] Volume ratio of NiO and YSZ; NiO:YSZ = 50:50.
[c] Weight ratio of LSCF-GDC; LSCF:GDC = 50:50.

Cell	Operating temperature	OCV (V) Experimental	OCV (V) Calculated	j (mA cm^{-2}) at 0.7 V	P_{max} (mW cm^{-2}) at 0.5 V
SC_1300	650 °C	1.12	1.13	115	100
	700 °C	1.12	1.12	230	190
	750 °C	1.11	1.11	400	335
	800 °C	1.10	1.10	620	525
SC_1400	650 °C	1.13	1.13	160	135
	700 °C	1.12	1.12	310	260
	750 °C	1.11	1.11	500	430
	800 °C	1.10	1.10	770	675
DC_1300	650 °C	1.11	1.13	150	120
	700 °C	1.12	1.12	250	205
	750 °C	1.11	1.11	435	350
	800 °C	1.10	1.10	655	535
DC_1400	650 °C	1.13	1.13	185	160
	700 °C	1.13	1.12	320	280
	750 °C	1.12	1.11	525	460
	800 °C	1.11	1.10	795	695

Table 2. Experimental parameters obtained from the *j-V* curves

Cell	Operating temperature	R_{ohm} (Ω cm^2)	R_1 (Ω cm^2)	R_2 (Ω cm^2)	R_3 (Ω cm^2)	ASR (Ω cm^2)
SC_1300	700 °C	0.80(7)	0.34(6)	0.67(7)	0.91(3)	2.72(23)
	750 °C	0.53(2)	0.080(10)	0.33(2)	0.45(4)	1.39(18)
	800 °C	0.38(1)	0.020(4)	0.13(2)	0.34(5)	0.87(12)
SC_1400	700 °C	0.59(6)	0.30(7)	0.66(8)	1.05(8)	2.80(29)
	750 °C	0.29(4)	0.010(2)	0.41(7)	0.53(7)	1.24(18)
	800 °C	0.22(4)	0.009(1)	0.26(5)	0.32(6)	0.81(16)
DC_1300	700 °C	0.51(2)	0.056(9)	0.63(5)	1.27(6)	2.47(22)

	750 °C	0.35(2)	0.029(6)	0.39(7)	0.61(5)	1.38(20)
	800 °C	0.24(1)	0.007(2)	0.27(1)	0.46(1)	0.98(5)
DC_1400	700 °C	0.66(6)	0.010(4)	0.64(2)	0.57(2)	1.88(14)
	750 °C	0.47(1)	0.005(1)	0.36(2)	0.27(3)	1.11(6)
	800 °C	0.28(2)	0.005(1)	0.27(2)	0.22(3)	0.77(8)

Table 3. EIS parameters obtained from fittings using equivalent circuits